

Article

The Role of Mineral Assemblages in the Environmental Impact of Cu-Sulfide Deposits: A Case Study from Norway

Yulia Mun ^{1,*}, Sabina Strmić Palinkaš ¹ and Kåre Kullerud ²

¹ Department of Geosciences, UiT The Arctic University of Norway, Hansine Hansens veg 18, 9019 Tromsø, Norway; sabina.s.palinkas@uit.no

² Norwegian Mining Museum, Hyttegata 3, 3616 Kongsberg, Norway; kk@bvm.no

* Correspondence: Yulia.mun@uit.no; Tel.: +47-483-30-892

Abstract: Metallic mineral deposits represent natural geochemical anomalies of economically valuable commodities but, at the same time, their weathering may have negative environmental implications. Cu-sulfide mineral deposits have been recognized as deposits with a particularly large environmental footprint. However, different Cu deposits may result in significantly different environmental impacts, mostly depending on weathering conditions, but also on geological characteristics (mineralogy, geochemistry, host-rock lithology) of the Cu mineralization. This study presents new mineral and geochemical data from the Repparfjord Tectonic Window sediment-hosted Cu deposits and the Caledonian volcanogenic massive sulfides (VMS) deposits. The deposits share similar mineral features, with chalcopyrite and bornite as the main ore minerals, but they differ according to their trace element composition, gangue mineralogy, and host lithology. The studied sediment-hosted Cu deposits are depleted in most toxic metals and metalloids like Zn, As, Cd, and Hg, whereas the Røros Caledonian VMS mineralization brings elevated concentrations of Zn, Cd, In, Bi, As, and Cd. The conducted leaching experiments were set to simulate on-land and submarine weathering conditions. A high redox potential was confirmed as the main driving force in the destabilization of Cu-sulfides. Galvanic reactions may also contribute to the destabilization of minerals with low rest potentials, like sphalerite and pyrrhotite, even under near-neutral or slightly alkaline conditions. In addition, the presence of carbonates under near-neutral to slightly alkaline conditions may increase the reactivity of Cu sulfides and mobilize Cu, most likely as CuCO_3 (aq).

Keywords: Cu-sulfide ore; Nussir; Ulveryggen; Røros VMS deposit; leaching tests; submarine weathering conditions; on-land weathering conditions

Citation: Mun, Y.; Strmić Palinkaš, S.; Kullerud, K. The Role of Mineral Assemblages in the Environmental Impact of Cu-Sulfide Deposits: A Case Study from Norway. *Minerals* **2021**, *11*, 627. <https://doi.org/10.3390/min11060627>

Academic Editor: Carlito Tabelin, Kyoungeun Yoo and Jining Li

Received: 31 May 2021

Accepted: 9 June 2021

Published: 12 June 2021

Publisher's Note: MDPI stays neutral with regard to jurisdictional claims in published maps and institutional affiliations.



Copyright: © 2021 by the authors. Licensee MDPI, Basel, Switzerland. This article is an open access article distributed under the terms and conditions of the Creative Commons Attribution (CC BY) license (<http://creativecommons.org/licenses/by/4.0/>).

1. Introduction

Copper is one of the most widely used mineral commodities in modern society, with a particular importance to electronics, electrical power generation, and the renewable energy sector, as well as in electric vehicle technologies [1–3]. In nature, Cu can be found in various types of mineral deposits, but in addition to the Cu-porphyry type (e.g. Chuquibambilla, Chile [4]; El Teniente, Chile [5]; Ok Tedi, Papua New Guinea [6]), deposits of volcanogenic massive sulfides (VMS) and Cu-sediment hosted types represent the most important sources of Cu. Worldwide, 20 million tons (Mt) of copper was the total mine production in 2020 [7]. This number decreased from 24.5 Mt in 2019 due to COVID-19 lockdowns in April and May [8]. Chile remains the major copper producer (5.7 Mt) followed by Peru (2.2 Mt), China (1.7 Mt), DR Congo (1.3 Mt), and the US (1.2 Mt) [9]. A range from 60% to 75% of copper is mined from porphyry-copper deposits [10], 20% from sediment-hosted Cu deposits [11], and around 6% of Cu is mined from VMS deposits [12].

In this study, sediment-hosted Cu mineralization is represented by samples from the Nussir and Ulveryggen Cu deposits, from the Repparfjord Tectonic Window, while the Røros deposit, located within the Upper Allochthon of Scandinavian Caledonides, was

selected as representative of VMS mineralization (Figure 1). All three deposits are characterized by chalcopyrite and bornite as the main ore minerals, but they significantly differ in trace element composition, gangue mineralogy, and host lithology. The Ulveryggen Cu sediment-hosted deposit was mined in the period from 1972 to 1978/79, and tailings were deposited subaqueously in Repparfjorden. The Nussir deposit has not been mined yet, but there are plans for start-up mining of both the Nussir and Ulveryggen deposits in the near future [13]. The mine tailings from this operation are designated to be disposed of subaqueously in Repparfjorden as well. The Røros VMS deposit was mined from 1644 to 1977 [14], and similar to other historic VMS mines along the Scandinavian Caledonides, the mine waste material was disposed of on land, and still represents a significant environmental threat [15].

Mining activities may result in negative environmental impacts due to the accumulation of large quantities of mine waste material, generation of acid mine drainage (AMD), and dispersion of heavy metals in aquifers, streams, and marine sediments and soils. Copper has been recognized as a commodity with a particularly large environmental footprint (e.g. [16–18]); the environmental impact of Cu mines mostly depends on tailings disposal site conditions and the geological features of Cu mineralization, including mineral, geochemical, and host lithology characteristics (e.g. [19–22]).

AMD is a major problem associated with mineral deposits, in which Cu occurs in the form of sulfides (e.g. chalcopyrite, bornite, chalcocite, covellite) or if barren sulfides (e.g. pyrite, marcasite, pyrrhotite) represent a significant component in the ore mineral assemblage (e.g. [23,24]). The consequences are often severe, leading to a lowering of the pH of contaminated aquifers, and release of metals and metalloids into the environment (e.g. [25–29]). Traditionally, tailings have been deposited in subaerial conditions, but several countries including Norway, practice subaqueous deposition [30]. Since subaqueous deposition in particular raises environmental concerns, we have tested the stability of representative Cu mineral assemblages from two of the most common types of Cu-sulfide deposits in Norway (sediment-hosted Cu deposits and VMS deposit) in a set of experiments that simulated subaerial and subaquatic weathering site conditions.

Kinetic leaching tests represent a powerful and relatively inexpensive tool to predict generation of AMD (e.g. [31]). They are designed to simulate sulfide-weathering processes in different physicochemical conditions. Kinetic leaching tests can be industrial or performed in the laboratory. Industrial tests are run in leaching columns, heaps, tanks, vats, dumps, large bins or drums [32]. They are placed in the field and subjected to meteoric waters, oxygen from the atmosphere, and changing temperature depending on the season. These tests can be conducted for several months to several years and are infrequently sampled for concentrations of dissolved metals and metalloids, sulfate, and changing pH and Eh parameters [33]. The tests can be accelerated by adding additional water [32].

However, more often the leaching tests are performed in miniature versions and run in laboratory size equipment—batch reactors, leaching columns, and humidity cells (e.g. [34–42]). The results are later extrapolated or mathematically modelled for larger volumes [33]. The tests are well-controlled and parameters such as water pH and Eh, metals and metalloids concentrations are continuously measured. The tests are often accelerated by increased temperature or the addition of hydrogen peroxide (e.g. [43]). The laboratory leaching tests also allow determination of an acid neutralizing capacity of gangue minerals and the acid producing potential of sulfides as well as to test remediation mechanisms, (e.g. [34,44–46]). However, many authors (e.g. [47]) argue that laboratory tests cannot be simply extrapolated to the field conditions. For example, a faster oxidation of pyrite and chalcopyrite from the Aitik site in Northern Sweden was observed in the laboratory compared to the field conditions [47].

The importance of characterization of ore parageneses and their host rocks was recognized as an important tool in the prediction of leaching of heavy metals from naturally contaminated rocks during anthropogenic activities e.g. underground constructions [31].

The tests are designed around primary ore mineralization to observe the oxidation potential of major ore minerals, and aim to extrapolate the results of the study to apply to produced mine tailings. The reactivity of the tailings with the surrounding environment will be significantly higher due to particle size and an increase in surface energy.

Norway has a long shoreline, and the ore-bearing rocks are often subjected to weathering by seawater. In addition, Norway is one of few countries where subaquatic mine tailings deposition is permitted. In both cases, it is important to understand the role of salinity on weathering of sulfides. Therefore, during the experiments seawater was used together with meteoric water.

The aim of this study is to evaluate the potential environmental impact of the studied Cu mineralization, considering geological characteristics including mineralogy, geochemistry, as well as the main physicochemical features of subaerial and subaquatic disposal sites.

2. Geological Settings

2.1. *Sediment-Hosted Cu Deposits of Nussir and Ulveryggen, Repparfjord Tectonic Window*

The Repparfjord Tectonic Window, Northern Norway, is composed of mafic metavolcanics and carbonate-siliciclastic sequences that were compressed in a SE-NW direction during the Svecofennian Orogeny at ca. 1.84 Ga [48,49]. The rocks are metamorphosed under greenschist to lower amphibolite facies conditions, and [50] determined the age of host volcanics to be about 2.1 Ga, with Nussir mineralization around 1.765 Ga. The Repparfjord Tectonic Window contains numerous sites with Cu mineralization (e.g. [14,51]), of which the Nussir (26.7 Mt at 1.13% Cu) and the Ulveryggen (7.7 Mt at 0.81% Cu) deposits have the greatest implications for the local environment [14,52]. The Nussir deposit is hosted by a thin (no more than 5 m thick) metadolostone layer that can be traced for several kilometres (Figure 1a,c), intercalated with metasandstone, metasilstone and metapelites. The metasedimentary complex is overlain by a several hundred meters thick metavolcanic sequence [49,50,53]. Despite the close geographical occurrence of the Nussir and Ulveryggen deposits, they have different lithologies. The Ulveryggen deposit is hosted by arkosic metasandstones, metasilstones, and metaconglomerates with low carbonate content. Mineralization can be traced for more than 1 km in the northeast direction and is structurally confined to tight folds [48,49,54,55]. Chalcopyrite, bornite, sphalerite, and minor pyrite are the main ore minerals at both deposits.

The Nussir mineralization is confined to a thin (up to 5 m thick) dolomitic marble layer intercalated with metasilstone, metapelites and metasandstones, localizing the mineralization within quartz-carbonate veins as well as disseminated in mafic metavolcanics [49,50,54,55]. The major ore minerals at the Nussir and Ulveryggen deposits are chalcopyrite, bornite, and chalcocite [49,50,54].

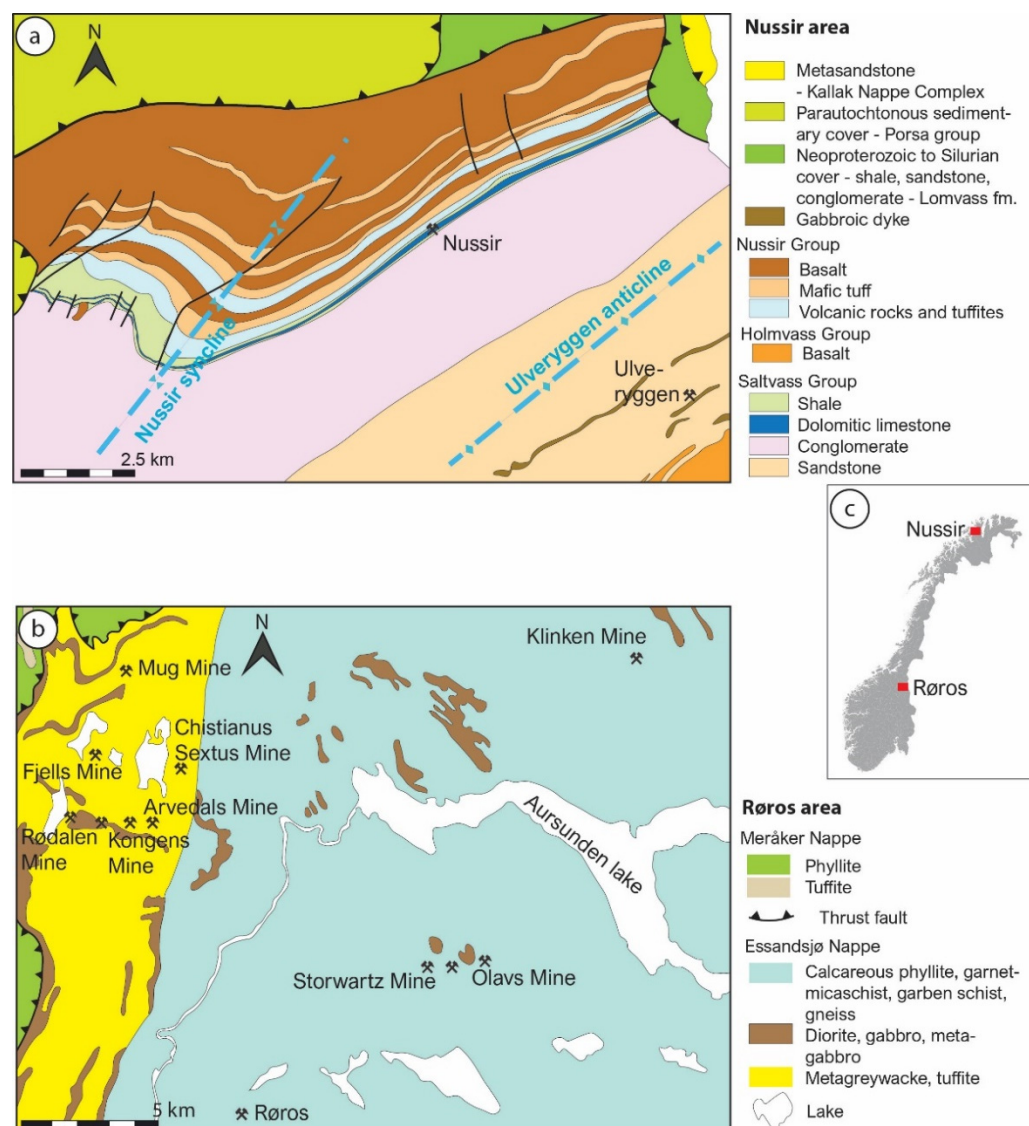


Figure 1. Geological maps showing the locations of the mines in (a) the Repparfjord Tectonic Window: Nussir and Ulveryggen sediment-hosted Cu deposits, and (b) the Røros area, drawn based on interactive online maps at [56] as well as modified after [49,55]. The map of Norway in (c) shows the locations of the Nussir, and Røros areas.

2.2. Volcanogenic Massive Sulfide (VMS) Deposit Røros, The Upper Allochthon of Scandinavian Caledonides

The Røros VMS mining area includes several hundreds of mineralizations in the south-eastern part of the Upper Allochthon of the Scandinavian Caledonides [57], including the Røros deposit studied herein. The mineralizations are characterized by predominately chalcopyrite, sphalerite, pyrite, and galena hosted by interbedded metatuffite, metagraywacke, and gabbroic sills and dykes [14,58,59].

The Upper Allochthon of Scandinavian Caledonides extends for about 1500 km, from the Stavanger region in southern Norway to the Barents Sea region in northern Norway. This first-order tectonostratigraphic unit is dominated by sedimentary and magmatic rocks derived from the Iapetus Ocean, including ophiolite and island-arc complexes usually associated with VMS type mineralization (Figure 1b,c; [60–62]).

The Røros mining area in Trøndelag County, south-eastern Norway, hosts numerous occurrences of the VMS type (Figure 1b). Among the largest occurrences are found at the Storwartz and Olav mines in the eastern sector, and the Kongens mine in the north-west-

ern sector (Figure 1), with average Cu and Zn contents of about 2.7% and 4.2–5%, respectively [59]. The mineralization is hosted by metagraywacke interbedded with metatuffites, metabasalts and gabbroic sills and dykes [14,58,59], with major ore minerals: chalcopyrite, pyrrhotite, sphalerite, and pyrite.

3. Materials and Methods

For this study, representative samples of the Cu sulfide mineralization were selected from the Nussir and Ulveryggen sediment-hosted Cu deposits, and from the Røros VMS deposit. Two main types of samples were analyzed: (1) Mineral assemblages composed of ore and gangue minerals and (2) Individual Cu-sulfide minerals.

Twenty-seven polished thin sections of representative mineral assemblages were prepared at the Department of Geosciences at UiT The Arctic University of Norway. Three thin sections represented reference samples for the respective deposits. The reference samples were studied under a reflective polarizing light microscope and a Zeiss Merlin Compact Field Emission Scanning Electron Microscope (FE-SEM) equipped with an energy-dispersive X-ray spectrometer (EDS) at UiT The Arctic University of Norway, to determine mineral and geochemical characteristics of the ore mineral assemblages prior to and after the leaching tests. In order to investigate the primary ore, the SEM was run in a high vacuum regime at 20 kV accelerating voltage, 20 s counting time, and with an aperture of 60 μm .

In order to simulate weathering processes corresponding to the tailings disposal site conditions, a set of leaching experiments were performed on the polished thin sections (Figure 2). The experiments were designed to simulate (Figure 3): (1) Subaquatic vs. on-land disposal site conditions; (2) Oxidative vs. reductive conditions; (3) Carbonate buffered vs. carbonate free systems; and (4) Seawater infiltrated vs. meteoric water infiltrated sites (Table 1). Each thin section was placed in an individual beaker of 400 mL with a height of 10.5 cm and diameter of 8.5 cm. The thin sections were then covered with a 4 cm thick layer of quartz sand (200 g) for the simulations of on-land conditions, whereas natural marine sediments (200 g) were used for the simulations of submarine conditions.

The average organic content in the natural marine sediments was 0.82 wt.% (Supplementary Table S1), whereas the quartz sand was free of organic matter. To test the influence of redox potential, half of the beakers with quartz sand were doped with ~10 wt.% of organic matter and sealed with parafilm tape to prevent oxidation reactions. The other half of the beakers were left open during the entire experiment and refilled with circa 150 mL of meteoric water once per day to ensure oxidative conditions. Pure calcium carbonate was used to buffer relevant solutions. The experiments were run for three months, and in order to accelerate the reactions, the beakers were kept in a water bath at 50 °C.

At the end of the experiments, the samples were carefully removed and investigated under a reflective light microscope. The formation of secondary minerals was studied by Raman spectroscopy, conducted at UiT The Arctic University of Norway in Tromsø. A Renishaw inVia confocal Raman microscope equipped with a 532 nm (green) diode laser was used to identify the mineral phases in the studied ore samples, as well as the degree of weathering after simulation of weathering conditions under on-land and subaquatic conditions. The identification was based on Raman spectra published in the literature [63].

Individual grains of Cu sulfides were handpicked under a binocular microscope, washed in an ultrasonic bath and pulverized in an agate mortar. An amount of 0.5 g was analyzed for bulk trace element composition at the AcmeLabs (Vancouver, B.C. Canada), on an ICP MS instrument following the internal LF202 analysis code.

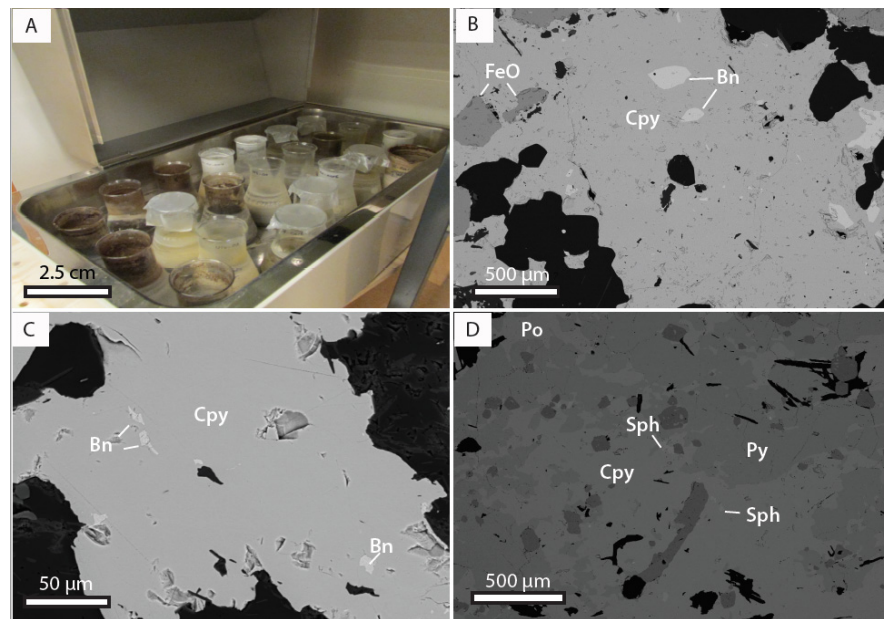


Figure 2. (A) Photograph of the test setup; (B) backscattered electron image of chalcopyrite (Cpy) in assemblage with bornite (Bn) and inclusions of iron oxides (FeO) from unaltered reference sample E-N-1 (Nussir); (C) backscattered electron image of chalcopyrite (Cpy) with small inclusions of bornite (Bn) from unaltered reference sample E-U-1 (Ulveryggen); (D) backscattered electron image of the Røros reference sample E-R-1 showing the mineral assemblage of chalcopyrite (Cpy), sphalerite (Sph), pyrite (Py), and pyrrhotite (Po).



Figure 3. Schematic presentation of test settings #1–#8 conditions. Eh and pH are measured in sediments before the tests. See text for explanation.

Table 1. Experimental setups. The cross mark corresponds to the ingredient added to the composition of the mixture. Sample last digits correspond to the experiment setup number.

Sample #	Condition #	Condition Description	Materials Used to Maintain the Designed Conditions					
			Marine Sediment	Prefabricated Sand	Sea Water	Meteoric Water	Organic Matter	Carbonate
Env- ¹ NS-1	1	Marine sediments, TOC = 0.82 wt.%. Carbonate buffered Seawater	+		+			+
Env- ² Ulv-1			+		+			+
Env- ³ RS-1			+		+			+
Env-NS-2	2	Marine sediments, TOC = 0.82 wt.%. Carbonate buffered Meteoric water	+			+		+
Env-Ulv-2			+			+		+
Env-RS-2			+			+		+
Env-NS-3	3	Marine sediments, TOC = 0.82 wt.%, non-buffered. Seawater	+		+			
Env-Ulv-3			+		+			
Env-RS-3			+		+			
Env-NS-4	4	Marine sediments, TOC = 0.82 wt.%, non-buffered. Meteoric water	+			+		
Env-Ulv-4			+			+		
Env-RS-4			+			+		
Env-NS-5	5	Quartz sand, TOC=0 wt.%, carbonate-buffered. Meteoric water		+		+		+
Env-Ulv-5				+		+		+
Env-RS-5					+		+	+
Env-NS-6	6	Quartz sand, TOC=0 wt.%, non-buffered. Meteoric water		+		+		
Env-Ulv-6				+		+		
Env-RS-6					+		+	
Env-NS-7	7	Quartz sand, TOC=10 wt.%, carbonate-buffered. Meteoric water		+		+	+	+
Env-Ulv-7				+		+	+	+
Env-RS-7					+		+	+
Env-NS-8	8	Quartz sand, TOC=10 wt.%, non-buffered. Meteoric water		+		+	+	
Env-Ulv-8				+		+	+	
Env-RS-8					+		+	

¹ NS—Nussir; ² Ulv—Ulveryggen; ³ RS—Røros, “+” — present in the experiment

4. Results

4.1. Mineral Analyses

4.1.1. Nussir and Ulveryggen

Mineral analyses show that typical ore assemblages from the Nussir and Ulveryggen sediment hosted Cu deposits consist of chalcopyrite, bornite, and chalcocite (Figure 2B, C). The Røros VMS mineralization is represented by massive sulfide bodies predominantly composed of chalcopyrite, sphalerite, pyrite and pyrrhotite (Figure 2D).

The Nussir dolomitic marble contains rhomboidal-shaped fragments of carbonates that are up to 5 mm in diameter. The mineralization is confined to crosscutting quartz-carbonate veins with euhedral to subhedral grains of vein carbonate, which are up to 0.1–

0.3 mm in diameter. Quartz grains are anhedral and about 0.1 mm in diameter. Chalcopyrite is the dominant Cu mineral together with bornite; the minerals are intergrown and contain abundant inclusions of pyrite and sphalerite (Figure 2B).

The Ulveryggen arkosic metasandstone contains fragments of quartz and feldspar up to 0.2 mm in size. The ore minerals are disseminated and they have grown interstitially between fragments of quartz and feldspar together with muscovite. The main ore minerals are bornite and chalcopyrite (Figure 2C), with minor amounts of pyrite and chalcopyrite.

4.1.2. Røros

Since the Røros samples were prepared from pieces of massive ore, only ore minerals were observed under the microscope. The main ore minerals are pyrrhotite, pyrite, chalcopyrite and sphalerite, which show various intergrowth textures. Chalcopyrite, which is the most abundant mineral, occurs as individual grains that are several centimetres in diameter. Pyrite and pyrrhotite crystals also show large grain-sizes (several centimetres in diameter), while sphalerite forms small inclusions of less than 0.1 mm in diameter (Figure 2D).

4.2. Leaching Tests

Experimental conditions #1 (Marine sediments, TOC = 0.82 wt.%; carbonate buffered; infiltrated with seawater (Figure 3); $Eh_{sed} = 239.7$ mV, $pH_{sed} = 7.64$, where Eh_{sed} and pH_{sed} are values of redox potential and pH for pore water in sediments measured after initial stabilization of conditions, i.e. 60 h after the experiment started) did not affect stability of mineral assemblages from the Nussir and Ulveryggen deposits (Figures 4A and 5A). However, for the sample from the Røros VMS deposit, small grains of sphalerite were weathered while some pyrite grains remained well-preserved (Figure 6A; Supplementary Figures S3H and S4A,B).

Experimental conditions #2 (Marine sediments, TOC = 0.82 wt.%; carbonate buffered; infiltrated with meteoric water; $Eh_{sed} = 247.9$ mV, $pH_{sed} = 7.31$; Figure 3) resulted in partial oxidation of sulfides from the Nussir and Ulveryggen deposits (Figures 4 and 5B; Supplementary Figures S1A–C and S2B). As for the experimental conditions #1, small grains of sphalerite from the Røros VMS deposit were affected (Figure 6B; Supplementary Figure S4D). Pyrite was partly oxidized along rims, while other parts remained unaltered (Figure 6B; Supplementary Figure S4C–E). Pyrrhotite was weathered significantly (Supplementary Figure S4D), and chalcocite was weathered while chalcopyrite remained unaltered (Supplementary Figures S4C,E).

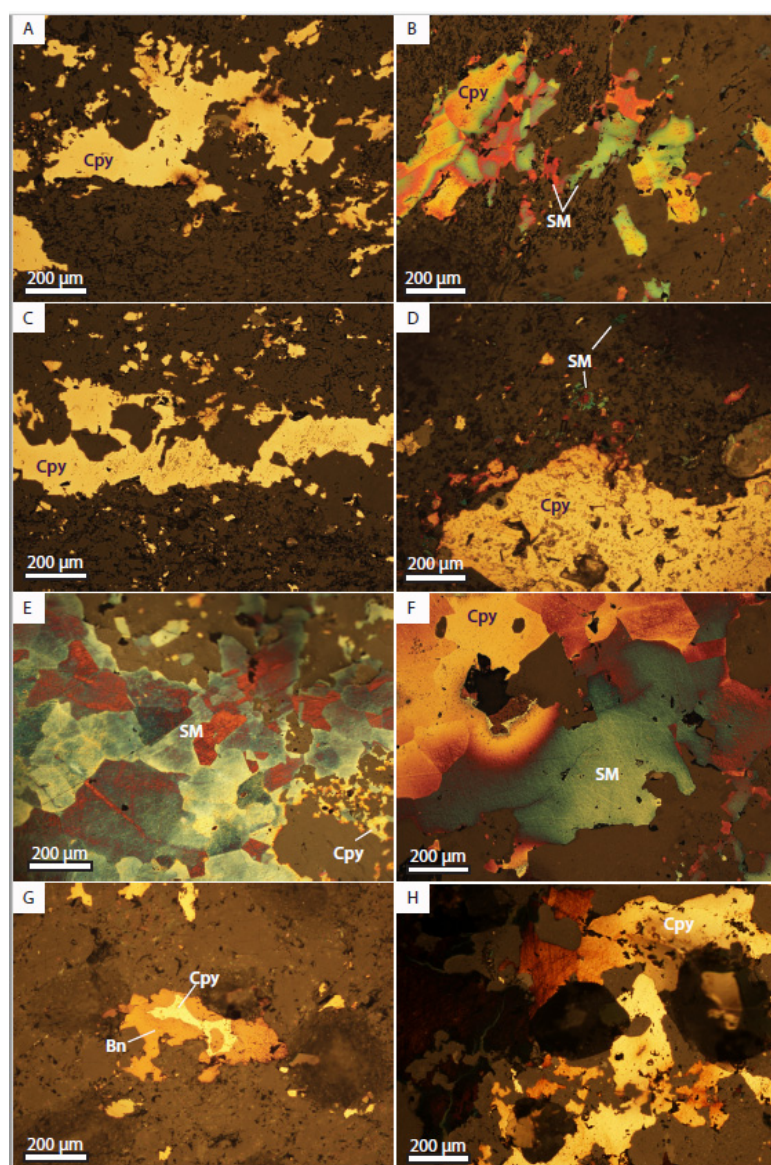


Figure 4. Microphotographs of samples under the reflected light microscope from the Nussir test runs after 90 days of the weathering experiment. The photographs are taken in crossed polars and correspond to test setups from 1 to 8 in Table 1. **(A)** reductive condition #1: well-preserved chalcopyrite (Cpy) grain (sample ENV-NS-1); **(B)** reductive condition #2: secondary minerals (SM) on top of chalcopyrite (Cpy) (sample ENV-NS-2d); **(C)** reductive condition #3: well-preserved chalcopyrite, secondary minerals are possibly forming in the cavities in the grain (Sample ENV-NS-3); **(D)** reductive condition #4: secondary minerals formed on the surface of chalcopyrite (Cpy, sample ENV-NS-4); **(E)** oxidative condition: secondary minerals on the surface of Cpy (ENV-NS-5); **(F)** oxidative condition #6: Cpy grain is partly oxidized (ENV-NS-6); **(G)** oxidative condition #7: well-preserved assemblage of Cpy and bornite (Bn) (ENV-NS-7); **(H)** oxidative condition #8: intensively oxidized chalcopyrite grain (#ENV-NS-8).

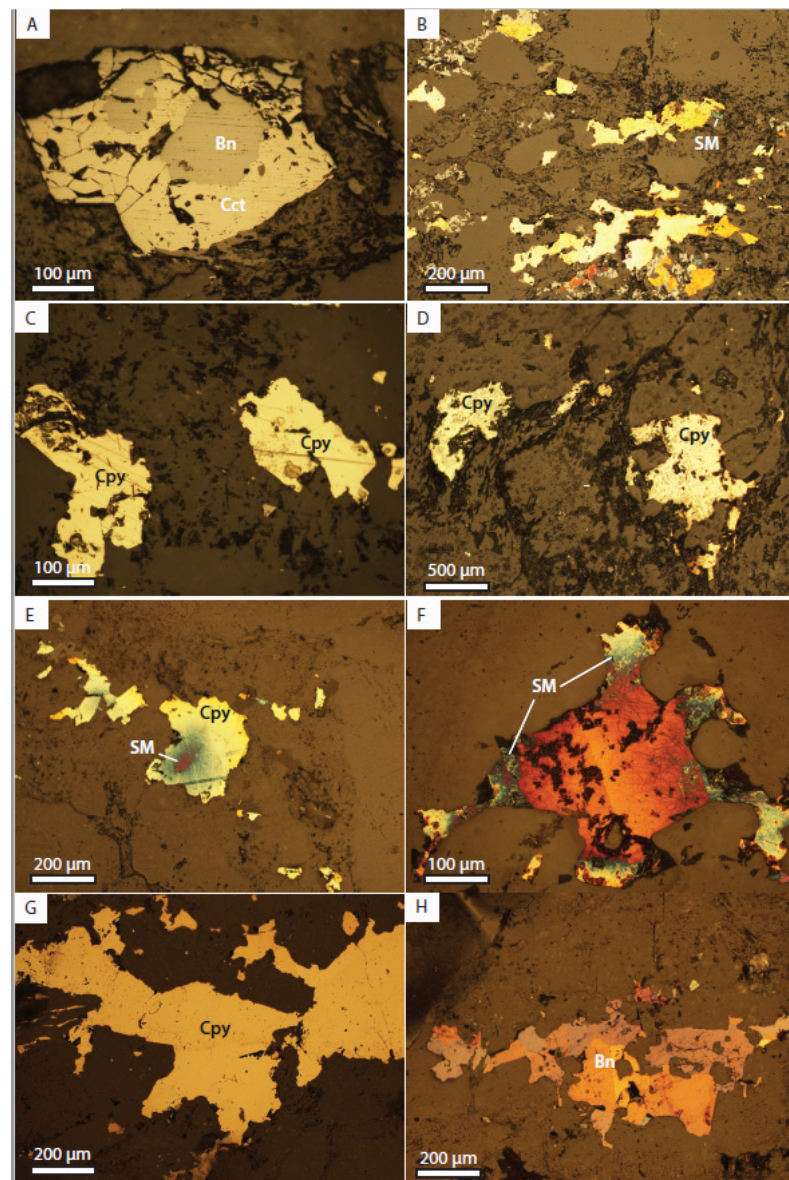


Figure 5. Microphotographs of Ulveryggen samples after 90 days of experiments. The photographs are taken under a reflected light microscope, with crossed polarizers. Setup description is given in Table 1, (A)–(H) microphotographs correspond to #1–8 conditions. (A) Intergrowth of chalcocite (Cct) with bornite (Bn, ENV-Ulv-1); (B) well-preserved chalcopyrite (Cpy) with minor oxidation of fine grains (ENV-Ulv-2); (C) well-preserved chalcopyrite grains (ENV-Ulv-3); (D) unaltered chalcopyrite grains (ENV-Ulv-4); (E) partly oxidized chalcopyrite grain with secondary mineral and oxidation cover on the surface; (F) oxidized Cu sulfide, likely chalcopyrite with secondary minerals formed on the lateral parts; (G) well-preserved chalcopyrite grain; and (H) micro-assemblage of well-preserved bornite (Bn) with chalcopyrite.

Experimental conditions #3 (Marine sediments, TOC = 0.82 wt.%; no added carbonates; infiltrated with seawater; $E_{h_{sed}} = 211.1$ mV, $pH_{sed} = 7.29$; Figure 3) did not affect the samples from the Nussir and Ulveryggen deposits (Figures 4C and 5C; Supplementary Figure S2D), but sulfides from the Røros VMS deposit went through extensive oxidation reactions (Figure 6C; Supplementary Figure S4F,G). Pyrrhotite was oxidized significantly, however chalcopyrite crosscutting pyrrhotite remained well-preserved (Figure 6C). Pyrite was partly oxidized along the rims. Covellite was observed along cracks in the pyrite.

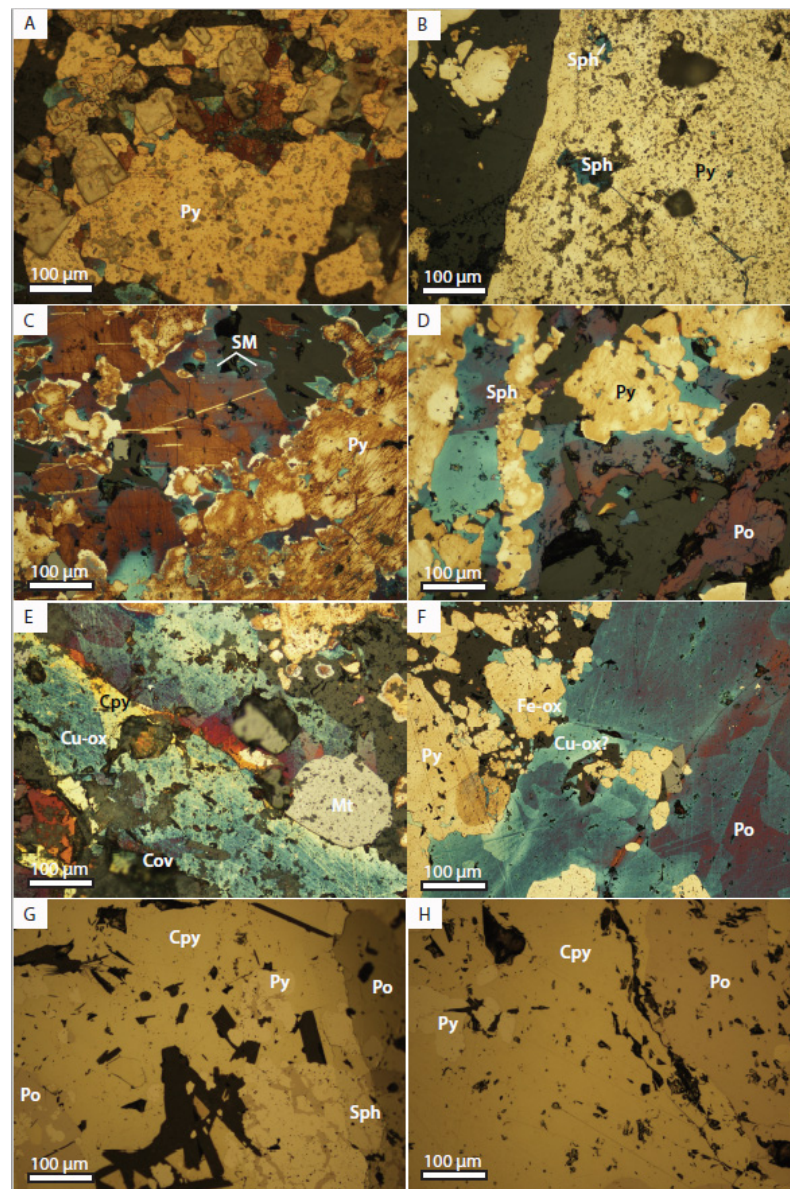


Figure 6. Microphotographs of polished thin sections from the Røros deposit after the 90-day experiment. The photographs (A)–(H) are taken under crossed poles, reflected light microscope and correspond to test conditions #1–8 (Table 1). (A,B) well-preserved pyrite grains (Py) with partly oxidized sphalerite (Sph) triangles (blue); (C) partly oxidized pyrite with secondary minerals formed on the rim of Cu-sulfides; (D) oxidation of sulfide mineral assemblages: pyrite (Py), sphalerite (Sph), pyrrhotite (Po), and secondary minerals likely formed on Cu-sulfides; (E) Intensive oxidation and the formation of secondary minerals (Cu-ox) of chalcopyrite (Cpy); (F) relatively well-preserved pyrite and intensely oxidized sphalerite, with minor amount of iron oxides (Fe-ox); (G,H) micro-assemblages of well-preserved sphalerite (Sph), chalcopyrite (Cpy), pyrite (Py), and pyrrhotite (Po).

Experimental conditions #4 (Marine sediments, TOC = 0.82 wt.%; no added carbonates; infiltrated with meteoric water; $Eh_{sed} = 231.2$ mV, $pH_{sed} = 7.63$; Figure 3) partly affected the Nussir and Ulveryggen samples: fine-grained fragments were significantly oxidized (Figures 4D and 5D; Supplementary Figures S1D–F and S2E), while larger grains were partly oxidized. Chalcopyrite obtained oxidized rims while bornite remained well-preserved (Supplementary Figures S1D–F and S2E). Chalcocite from the Nussir deposit was partly oxidized, while chalcocite in contact with pyrite from Ulveryggen remained well-preserved (Supplementary Figure S2E). The Røros samples were weathered significantly (Figure 6D; Supplementary Figure S4H). Notably, bornite was weathered to a

higher degree than chalcopyrite. The latter was found in veins within bornite and remained well-preserved (Supplementary Figure S4H). Oxidized rims were formed around pyrite grains, whereas pyrrhotite and sphalerite had undergone significant weathering (Figure 6F).

Experimental conditions #5 (quartz sand, TOC = 0 wt.%; carbonate buffered, infiltrated with meteoric water; $E_{h_{sed}} = 222.6$ mV, $pH_{sed} = 8.76$; Figure 3) affected the sulfides from all three studied deposits to different degrees. Chalcopyrite and bornite from Nussir were extensively weathered (Figure 4E; Supplementary Figure S1G), whereas for the Ulveryggen sample, chalcopyrite and chalcocite were partly weathered while most of the pyrite and bornite remained well-preserved (Figure 5E; Supplementary Figures S2F–H and S3A). Sulfides from Røros were more oxidized in comparison to sulfides from Nussir and Ulveryggen. In contrast to pyrite and chalcopyrite, which remained well-preserved or only partly oxidized, pyrrhotite and sphalerite were significantly weathered (Figure 6E; Supplementary Figure S5A–C).

Experimental conditions #6 (quartz sand, TOC = 0 wt.%; no added carbonates; infiltrated with meteoric water; $E_{h_{sed}} = 245.7$ mV, $pH_{sed} = 7.54$; Figure 3) resulted in extensive oxidation of the sulfides from the Nussir and Ulveryggen deposits. Chalcopyrite, bornite and chalcocite obtained a weathered rim around the grains (Figures 4F and 5F; Supplementary Figures S1H and S3B,C). Some grains of chalcopyrite were entirely covered with a thin film of weathering products (Figure 4F). Pyrite from Ulveryggen remained well-preserved, but might have accelerated the oxidation of bornite (Supplementary Figure S3C). Pyrrhotite and sphalerite from the Røros deposit were significantly weathered, whereas pyrite remained relatively well-preserved with insignificant formation of iron oxides (Figure 6F; Supplementary Figure S5D). A weathered Cu-containing mineral was also observed within the pyrite (Supplementary Figure S5D).

Experimental conditions #7 (quartz sand, TOC \approx 10 wt.%, carbonate buffered, infiltrated with meteoric water; initial $E_{h_{sed}} = 191.5$ mV, $pH_{sed} = 7.86$; Figure 3) did not affect the Nussir and Ulveryggen sulfides. The minerals remained well-preserved (Figures 4G and 5G; Supplementary Figure S3D,E). The Røros ore minerals also remained almost unaffected, however some pyrite grains were slightly tarnished with bright blue secondary covellite and brownish iron hydroxides (Figure 6G; Supplementary Figure S5E,F).

Experimental conditions #8 (quartz sand, TOC \approx 10 wt.%, no added carbonates, infiltrated with meteoric water; $E_{h_{sed}} = 286.1$ mV, $pH_{sed} = 5.43$; Figure 3) resulted in well-preserved sulfides from the Ulveryggen and Røros deposits (Figures 5H and 6H; Supplementary Figures S3F,G, and S5G). Chalcopyrite from Nussir was observed both as relatively well-preserved grains (Figure 4H) and significantly weathered grains (Supplementary Figure S2B).

4.3. Raman Spectroscopy

Raman spectra (Figure 7) obtained from chalcopyrite and pyrite from the Nussir, Ulveryggen, and Røros deposits suggest formation of new peaks 450 and 500 cm^{-1} after exposing samples from the Nussir and Ulveryggen to experimental conditions #2 and #5, respectively (Figure 7A–D).

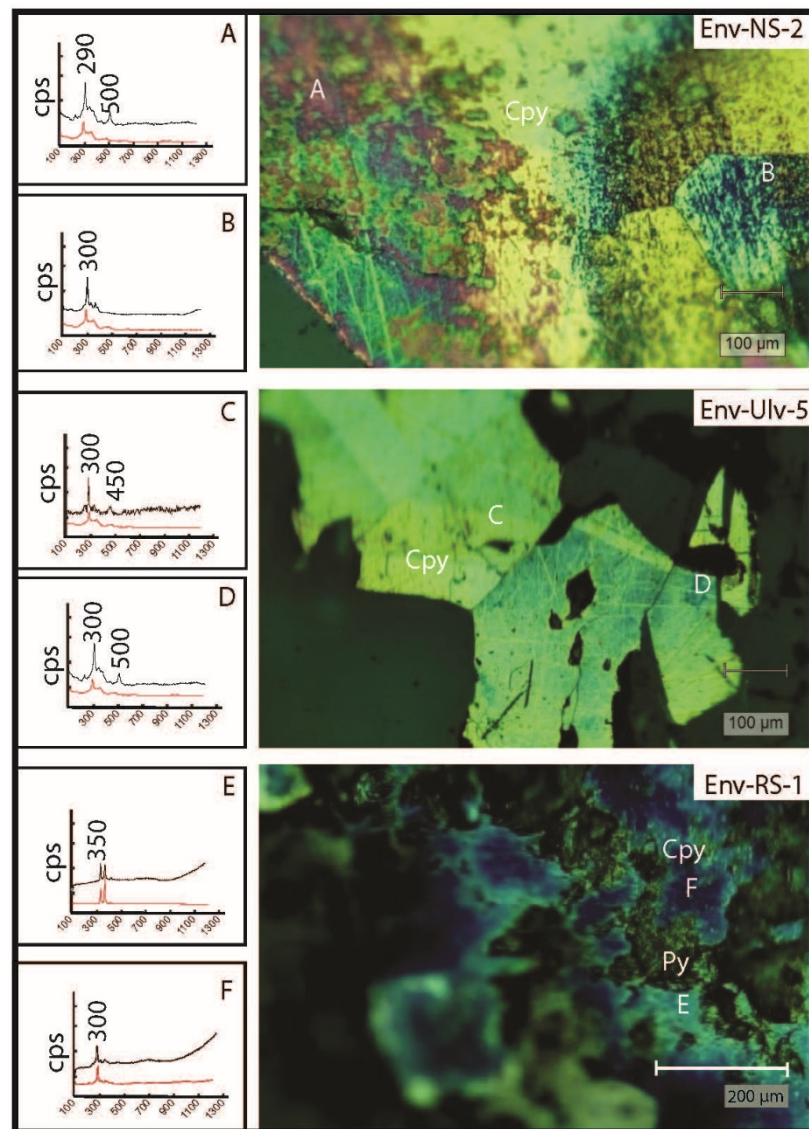


Figure 7. Raman spectrometry of chalcopyrite (Cpy) and pyrite (Py) from Nussir, Ulveryggen and Røros after 90-days of testing in selected conditions. Sample numbers correspond to condition numbers and can be found in Table 1. Cps—counts per second. **A–E:** right images are microphotographs of samples under reflected light microscope; left diagrams relate to Raman spot analyses. **A,B**—chalcopyrite (Cpy) from the Nussir deposit (sample Env-NS-2, experimental condition #2); **C,D**—chalcopyrite (Cpy) from the Ulveryggen deposit (sample Env-Ulv-5, experimental condition #5); **E**—pyrite (Py) and **F**—chalcopyrite (Cpy) from the Røros deposit (sample Env-RS-1, experimental condition #1).

4.4. Mineral Chemistry

In addition, to determine the concentration of potentially toxic elements including Cu, Zn, Ni, Hg, Cd, and As (e.g. [64]), the bulk chemical compositions of hand-picked Nussir, Røros chalcopyrite as well as Ulveryggen bornite were analyzed (Table 2). The Nussir and Ulveryggen results are taken from [53].

Table 2. Litho-geochemistry of hand-picked chalcopyrite from the Nussir deposit (NS-35-ccp), bornite from the Ulveryggen deposit (Ulv-2-bn) and chalcopyrite Røros Mine (RSL-ccp).

Element, ppm	LD	¹ NS-35-ccp	² Ulv-2-bn	³ RSL-ccp
Ag	0.5	0.5	LLD	>100
As	5	LLD	LLD	226.1
Ba	3	12	527	18
Bi	0.1	0.3	0.1	9.9
Cd	0.1	LLD	LLD	30
Co	1	85	2	535.9
Cu	10	>10,000	>10,000	>10,000
Hg	0.01	LLD	LLD	4.59
Mo	2	LLD	5	6.5
Ni	0.1	100	LLD	7.8
Pb	5	LLD	LLD	196.1
Rb	1	LLD	24	2.5
Sb	0.2	LLD	LLD	1.8
Sn	1	LLD	LLD	8
Tl	0.05	3.69	0.96	2
V	5	5	27	LLD
W	0.5	0.6	LLD	0.7
Zn	30	310	LLD	2942

¹ NS—Nussir, ² Ulv—Ulveryggen, ³ RSL—Røros; Bn—bornite, ccp—chalcopyrite, LD—limit of detection, LLD—lower than limit of detection, ND—no data.

4.4.1. Nussir and Ulveryggen

The Nussir chalcopyrite contains 100 ppm of Ni, 85 ppm of Co and 310 ppm of Zn. The content of Bi is 0.3 ppm, while As, Mo, Cd, Sb, Pb, and Hg contents are minor or below the detection limit. The Nussir chalcopyrite also contains Ba (12 ppm), most likely in the form of nearly insoluble inclusions of barite.

Ulveryggen bornite contains 2 ppm of Co and 5 ppm of Mo. Nickel, Zn, As, Sn, Sb, Cd, Pb, and Hg contents are minor or below the detection limit, while the Rb content is 24 ppm. The content of Ba in the Ulveryggen bornite is 527 ppm.

4.4.2. Røros

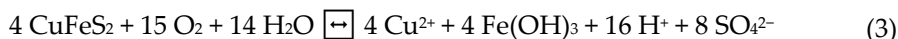
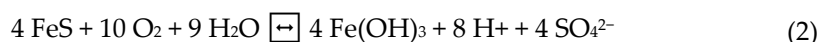
Chalcopyrite was picked from the crushed Røros sample. The Co content is 535.9 ppm. The chalcopyrite also contains: Ni 7.8 ppm and Zn 2942 ppm. As content is 226.1 ppm, and Sn and Sb contents are 8 and 1.8 ppm respectively. Chalcopyrite contains 30 ppm of Cd and 18 ppm of Ba. The Bi content is 9.9 ppm and Hg content is 4.59 ppm.

5. Discussion

The Cu mineralization found in the Nussir and Ulveryggen sediment-hosted Cu deposits is characterized by predomination of chalcopyrite, bornite and chalcocite. Mine tailings from these Cu-sulfide deposits are associated with a high risk for the generation of acid mine drainage (AMD) because of the high Fe²⁺/Fe³⁺ and S²⁻/SO₄²⁻ ratios in their mineral assemblages. Furthermore, the Ulveryggen deposit has a low carbonate content that additionally increases the risk. In contrast, a low content of potentially toxic elements such as As, Cd, Hg, and Zn in both, reduces their environmental threat [53].

The Røros Cu-Zn VMS deposit, similar to other VMS deposits worldwide [65,66], is characterized by a polymetallic composition (Table 2). The main ore minerals are sulfides, including chalcopyrite, bornite, pyrite, and pyrrhotite. High Fe²⁺ and S²⁻ contents together with an absence of carbonates from its mineral assemblages point to a high risk for the generation of AMD in this deposit (e.g. [23,27,46,67,68]). In addition, the enrichment in a wide spectrum of potentially toxic metals and metalloids (e.g. As, Bi, Cd, In, and Zn) magnifies the environmental risk associated with mining activities and/or processes of natural weathering in this type of ore deposits (e.g. Rio Tinto VMS deposits, the Iberian Pyrite Belt in Spain [26,28,69–71] and the Britannia Creek VMS deposit, Canada [48]).

Leaching tests are recognized as powerful tools to predict the behavior of sulfides in different conditions (e.g. [20,32,37,39,40]). Such tests play an important role in the initial phases of mining planning, while deciding the potential placement of tailings for future storage. The tests are usually performed in batch reactors specially equipped with sensors controlling temperature, pH, and the amount of dissolved oxygen (e.g. [39,47,72]). Otherwise, the tests can be performed in leaching columns (e.g. [32,73]) or in static conditions (e.g. [46,74]) for periods of several days to several years. The leaching experiments in this study were designed to test the stability of ore mineral parageneses from three different Cu deposits under diverse physicochemical conditions (Figure 3, Table 1), and predict the behavior of ore-bearing mineral assemblages disposed in on-land and submarine conditions. As expected, the high redox potential was the main driving factor in destabilization of sulfides (e.g. [75]):



The organic matter content of the natural marine sediments that were used (0.82 wt.%) was sufficient to prevent oxidation of the sulfides in experimental conditions in which the sulfide parageneses were exposed to seawater. In the setups with meteoric water, a different scenario was observed. A lower solubility of oxygen in seawater (4.6 mg/L at 50 °C) compared to meteoric water (5.6 mg/L at 50 °C) was probably one of the controlling factors [76]. When sediments were doped with an additional 10 wt.% of organic matter, the differences between seawater and meteoric water influence were not recorded.

The carbonate buffered conditions were mostly less reactive due to a slightly alkaline pH value of the infiltrating aqueous solutions. However, the samples from the Røros VMS deposit revealed that sphalerite can enter galvanic reactions and be extensively dissolved even in alkaline or near-neutral conditions. The prerequisite is that sphalerite (−0.24 V; [77]) occurs in direct contact with sulfides with greater rest potentials like pyrite (0.63 V; [78]) or chalcopyrite (0.54 V; [79]). In interactions with oxygen-rich solutions, sphalerite will act as an anode:



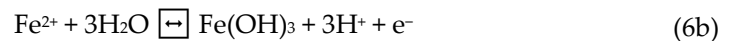
and prevent oxidation of pyrite, and Cu-sulfides reacting with oxygen adsorbed on their surface:



This reaction will not affect the pH of the aquifer, but it will promote leaching of Zn.

The galvanic reaction may represent a particularly large environmental issue in mineral deposits in which pyrrhotite (−0.24 V; [77]) is intergrown or occurs in direct contact with Cu-sulfides and/or pyrite:





The anode reaction will result in dissolution of pyrrhotite, oxidation of ferrous to ferric ions, and consequently in acidification of the system.

In the experimental setups buffered with carbonates, the Cu sulfides showed an increased reactivity (Figures 4B,E, 5B,E and 6E) whereas pyrite did not show significant changes under these conditions (Figure 6B). Carbonates are often used for prevention of acid mine drainage (e.g. [80]), but the results of this study show that in near-neutral to slightly alkaline conditions Cu can be mobilized from sulfides, most likely in the form of $\text{CuCO}_3(\text{aq})$ [53,81]. This reaction is more intensive in solutions with a higher redox potential (Figures 4E, 5E and 6E).

In addition, gangue mineralogy might also play a role in the rate and degree of oxidation. The Nussir mineralogy is hosted by dolomitic marble, while Ulveryggen Cu sulfides are hosted by arkosic sandstone, which retards the oxidation of sulfides [53]. Røros sulfides, studied here, were sampled from a massive ore with an absence of gangue minerals. Therefore, galvanic interaction was favoured to higher degree of oxidation and was not prevented or retarded by gangue mineralogy. Weathering in mine tailings will be accelerated due to higher surface area, however this is also true for gangue mineralogy which in the case of Nussir and Ulveryggen might play a buffering role. On the other hand Røros mineralization being hosted by massive mafic volcanic rocks, which are extremely soluble, will most probably not retard the oxidation reaction or buffer it to limited degree.

Raman spectroscopy confirmed the slight distortion of crystal lattices of pyrite and chalcopyrite (Figure 7), however, the signal was low. Optically, even when the blue tinge was observed in the Nussir and Ulveryggen samples, Raman analyses did not record any changes in crystal structure of sulfides from these two deposits. This is attributed to oxidation occurring in a thin layer of secondary minerals, which tends to be amorphous and is characterized by the absence of a detectable lattice. In addition, the signal from primary minerals is significantly higher.

6. Conclusions

The mineral assemblages from all three studied deposits point to a high risk for generation of acid mine drainage due their high $\text{Fe}^{2+}/\text{Fe}^{3+}$ and $\text{S}^{2-}/\text{SO}_4^{2-}$ ratios. However, different ore-forming conditions of sediment hosted Cu deposits (Nussir and Ulveryggen) from conditions related to the formation of VMS deposits (Røros) resulted in contrasting behavior of the trace elements. As a consequence, the Nussir and Ulveryggen deposits are depleted in most potentially toxic elements, such as As, Cd, Hg, and Zn, whereas the Røros VMS mineralization is enriched in a wide spectrum of potentially toxic metals and metalloids, including As, Bi, Cd, In, and Zn.

The leaching experiments revealed the redox potential as the main factor that controls the stabilities of Cu-sulfides for both on-land as well as submarine conditions. Galvanic reactions may contribute to the destabilization of minerals with low rest potentials, like sphalerite and pyrrhotite, even under near-neutral or slightly alkaline conditions. The destabilization of pyrrhotite can have particularly negative environmental consequences due to the release of ferrous ions to an aquifer and acidification of the system as a result of oxidation of ferrous to ferric ions.

Although carbonates are often used for prevention of acid mine drainage, the presence of carbonates under near-neutral to slightly alkaline conditions may increase the reactivity of Cu sulfides and mobilize Cu, most likely in the form of $\text{CuCO}_3(\text{aq})$.

More complex ore minerals assemblages lead to deeper weathering in given conditions. Thus, Røros chalcopyrite were notably more altered than chalcopyrite from the Ulveryggen and Nussir deposits.

Supplementary Materials: The following are available online at www.mdpi.com/2075-163X/11/6/627/s1, Figure S1. Microphotographs demonstrating the Nussir sulfides reaction after 90-

day tests; Figure S2: Microphotographs taken under a reflected light microscope; Figure S3: Microphotographs taken under reflected light; Figure S4: Microphotographs of Røros samples under reflected light; Figure S5: Microphotographs of Røros samples under the reflected light microscope after 90-days of experimental tests; Table S1: Total organic carbon (TOC) of gravity core HH-12-002-MF-GC obtained from Repparfjord.

Author Contributions: Conceptualization, Y.M., S.S.P.; methodology, Y.M. and S.S.P.; validation, Y.M. and S.S.P.; formal analysis, Y.M. and S.S.P.; investigation, Y.M. and S.S.P.; resources, Y.M., S.S.P. and K.K.; data curation, Y.M., S.S.P. and K.K.; writing—original draft preparation, Y.M.; writing—review and editing, Y.M., S.S.P. and K.K.; visualization, Y.M. and K.K.; supervision, S.S.P. and K.K.; project administration, S.S.P. and K.K.; funding acquisition, K.K.. All authors have read and agreed to the published version of the manuscript.

Funding: This research was funded by Tromsø Fylkes Kommune and SINTEF through the PhD project of the first author, grant number RDA12/167. The publication charges for this article have been funded by a grant from the publication fund of UiT The Arctic University of Norway.

Acknowledgments: We are thankful to Carlito Tabelin, the Academic Editor of the special issue “Novel and Emerging Strategies for Sustainable Mine Tailings and Acid Mine Drainage Management” for constructive comments and suggestions that significantly improved the text. The authors are thankful to Kai Neufeld for the assistance with the SEM work. The laboratory staff of the Department of Geosciences, UiT, Trine Merete Dahl, Karina Monsen, Ingvild Hald are acknowledged for the efficient work and assistance in samples preparation and TOC analysis. Nussir ASA and in particular Øystein Rushfeldt is thanked for providing this research with study material. The authors thank Calvin Shackleton for correction of text.

Conflicts of Interest: The authors declare no conflict of interest.

References

- Gordon, R.B.; Bertram, M.; Graedel, T.E. Metal Stocks and Sustainability. *Proc. Natl. Acad. Sci. USA* **2006**, *103*, 1209–1214.
- Schlesinger, M.E.; King, M.J.; Sole, K.C.; Davenport, W.G. *Extractive Metallurgy of Copper*, 5th ed.; Elsevier: Oxford, UK, 2011; 472p.
- Elshkaki, A.; Graedel, T.E.; Ciacci, L.; Reck, B.K. Copper demand, supply, and associated energy use to 2050. *Global Environ. Chang.* **2016**, *39*, 305–315.
- Ossandón, C.G.; Fréaut, C.R.; Gustafson, L.B.; Lindsay, D.D.; Zentilli, M. Geology of the Chuquicamata mine: A progress report. *Econ. Geol.* **2001**, *96*, 249–270.
- Cannell, J.; Cooke, D.R.; Walshe, J.L.; Stein, H. Geology, mineralization, alteration, and structural evolution of the El Teniente porphyry Cu-Mo deposit. *Econ. Geol.* **2005**, *100*, 979–1003.
- Large, S.J.; Quadt, A.V.; Wotzlaw, J.F.; Guillong, M.; Heinrich, C.A. Magma evolution leading to porphyry Au-Cu mineralization at the Ok Tedi deposit, Papua New Guinea: Trace element geochemistry and high-precision geochronology of igneous zircon. *Econ. Geol.* **2018**, *113*, 39–61.
- Garside, M. Copper—Statistics & Facts. Available online: <https://www.statista.com/topics/1409/copper/> (accessed on 7 June 2021).
- Flanagan, D.M. *Mineral Commodity Summaries*; U.S. Geological Survey: Reston, VA, USA, 2021.
- Garside, M. Major Countries in Copper Mine Production Worldwide from 2010 to 2020. Available online: <https://www.statista.com/statistics/264626/copper-production-by-country/> (accessed on 7 June 2021).
- Mudd, G.M.; Jowitt, S.M. Growing global copper resources, reserves and production: Discovery is not the only control on supply. *Econ. Geol.* **2018**, *113*, 1235–1267.
- Pietrzyk, S.; Tora, B. Trends in global copper mining—A review. *Miner. Eng. Conf.* **2018**, *427*, 012002.
- Nicholas Lapan. Everything You Need to Know about VMS Deposits. *Vis. Capital.* **2019**. Available online: <https://www.mining.com/web/everything-need-know-vms-deposits/> (accessed on 7 June 2021).
- Nussir ASA, available online: www.nussir.no (accessed on 30 November 2020).
- Sandstad, J.S.; Bjerkgård, T.; Boyd, R.; Ihlen, P.; Korneliusen, A.; Nilsson, L.P.; Often, M.; Eilu, P.; Hallberg, A. Metallogenic areas in Norway. In *Mineral Deposits and Metallogeny of Fennoscandia*; Geological Survey of Finland: Espoo, Finland, 2012; Volume 53, pp. 35–138.
- Banks, D.; Younger, P.L.; Arnesen, R.T.; Iversen, E.R.; Banks, S.B. Mine-water chemistry: The good, the bad and the ugly. *Environ. Geol.* **1997**, *32*, 157–174.
- Dudka, S.; Adriano, D.C. Environmental impacts of metal ore mining and processing: A review. *J. Environ. Qual.* **1997**, *26*, 590–602.
- Bridge, G. The social regulation of resource access and environmental impact: Production, nature and contradiction in the US copper industry. *Geoforum* **2000**, *31*, 237–256.

18. Berrill, P.; Arvesen, A.; Scholz, Y.; Gils, H.C.; Hertwich, E.G. Environmental impacts of high penetration renewable energy scenarios for Europe. *Environ. Res. Lett.* **2016**, *11*, 014012.
19. Seal, R.R., II; Foley, N.K. (Eds.) *Progress on Geoenvironmental Models for Selected Mineral Deposit Types*; U.S. Geological Survey: Reston, VA, USA, 2002; pp. 2002–2195.
20. Parbhakar-Fox, A.K.; Edraki, M.; Walters, S.; Bradshaw, D. Development of a textural index for the prediction of acid rock drainage. *Miner. Eng.* **2011**, *24*, 1277–1287.
21. Dold, B.; Weibel, L. Biogeometallurgical pre-mining characterization of ore deposits: An approach to increase sustainability in the mining process. *Environ. Sci. Pollut. R.* **2013**, *20*, 7777–7786.
22. Anawar, H.M. Sustainable rehabilitation of mining waste and acid mine drainage using geochemistry, mine type, mineralogy, texture, ore extraction and climate knowledge. *J. Environ. Manag.* **2015**, *158*, 111–121.
23. Bussière, B. Acid mine drainage from abandoned mine sites: Problematic and reclamation approaches. In Proceedings of the International Symposium on Geoenvironmental Engineering, ISGE 2009, Hangzhou, China, 8 September 2009; pp. 111–125.
24. Simate, G.S.; Ndlovu, S. Acid mine drainage: Challenges and opportunities. *J. Environ. Chem. Eng.* **2014**, *2*, 1785–1803.
25. Braungardt, C.B.; Achterberg, E.P.; Elbaz-Poulichet, F.; Morley, N.H. Metal geochemistry in a mine-polluted estuarine system in Spain. *Appl. Geochem.* **2003**, *18*, 1757–1771.
26. Enspaña, J.S.; López Pamo, E.; Esther, S.; Aduvire, O.; Reyes, J.; Baretino, D. Acid mine drainage in the Iberian Pyrite Belt (Odiel river watershed, Huelva, SW Spain): Geochemistry, mineralogy and environmental implications. *Appl. Geochem.* **2005**, *20*, 1320–1356.
27. Akcil, A.; Koldas, S. Acid mine drainage (AMD): Causes, treatment and case studies. *J. Clean. Prod.* **2006**, *14*, 1139–1145.
28. Ayora, C.; Caraballo, M.A.; Macias, F.; Rötting, T.S.; Carrera, J.; Nieto, J.-M. Acid mine drainage in the Iberian Pyrite Belt: 2. Lessons learned from recent passive remediation experiences. *Environ. Sci. Pollut. Res.* **2013**, *20*, 7837–7853.
29. Kefeni, K.K.; Msagati, T.A.M.; Mamba, B.B. Acid mine drainage: Prevention, treatment options, and resource recovery: A review. *J. Clean. Prod.* **2007**, *151*, 475–493.
30. Dold, B. Submarine tailings disposal (STD)—A review. *Minerals* **2014**, *4*, 642–666.
31. Tabelin, C.B.; Igarashi, T.; Villacorte-Tabelin, M.; Park, I.; Einstin, M.O.; Ito, M.; Hiroyoshi, N. Arsenic, selenium, boron, lead, cadmium, copper, and zinc in naturally contaminated rocks: A review of their sources, modes of enrichment, mechanisms of release, and mitigation strategies. *Sci. Total Environ.* **2018**, *645*, 1522–1553.
32. Lottermoser, B. *Mine Wastes Characterization, Treatment and Environmental Impacts*, 3rd Ed.; Springer: Berlin/Heidelberg, Germany, 2010; 400p.
33. De Andrade Lima, L.R.P. A mathematical model for isothermal heap and column leaching. *Braz. J. Chem. Eng.* **2004**, *21*, 435–447.
34. Gottschalk, V.H.; Buehler, H.A. Oxidation of sulphides. *Econ. Geol.* **1912**, *7*, 15–34.
35. Cheng, C.Y.; Lawson, F. The kinetics of leaching covellite in acidic oxygenated sulphate-chloride solutions. *Hydrometallurgy* **1991**, *27*, 269–284.
36. Falk, H.; Lavergren, U.; Bergbäck, B. Metal mobility in alum shale from Öland, Sweden. *J. Geochem. Explor.* **2006**, *90*, 157–165.
37. Rzepka, P.; Walder, I.F.; Aagaard, P.; Bożęcki, P.; Rzepa, G. Sub-sea tailings deposition leach modelling. *Geol. Geophys. Environ.* **2014**, *40*, 123–124.
38. Tabelin, C.B.; Veerawattananun, S.; Ito, M.; Hiroyoshi, N.; Igarashi, T. Pyrite oxidation in the presence of hematite and alumina: I. Batch leaching experiments and kinetic modeling calculations. *Sci. Total Environ.* **2017**, *580*, 687–698.
39. Embile, R.F., Jr.; Walder, I.F. Galena non-oxidative dissolution kinetics in seawater. *Aquat. Geochem.* **2018**, *24*, 107–119.
40. Embile, R.F., Jr.; Walder, I.F.; Schuh, C.; Donatelli, J.L. Cu, Pb and Fe release from sulphide-containing tailings in seawater: Results from laboratory simulation of submarine tailings disposal. *Mar. Pollut. Bull.* **2018**, *137*, 582–592.
41. Huyen, D.T.; Tabelin, C.B.; Thuan, H.M.; Dang, H.D.; Truong, P.T.; Vongphuthone, B.; Kobayashi, M.; Igarashi, T. The solid-phase partitioning of arsenic in unconsolidated sediments of the Mekong Delta, Vietnam and its release under various conditions. *Chemosphere* **2019**, *233*, 512–523.
42. Tomiyama, S.; Igarashi, T.; Tabelin, C.B.; Tangviroon, P. Acid mine drainage sources and hydrogeochemistry at the Yatani mine, Yamagata, Japan: A geochemical and isotopic study. *J. Contam. Hydrol.* **2019**, *225*, 103502.
43. Silva, L.F.O.; Querol, X.; da Boit, K.M.; Fdez-Ortiz de Vallejuelo, S.; Madariaga, J.M. Brazilian coal mining residues and sulphide oxidation by Fenton’s reaction: An accelerated weathering procedure to evaluate possible environmental impact. *J. Hazard. Mater.* **2011**, *186*, 516–525.
44. Jambor, J.L.; Dutrizac, J.E.; Groat, L.A.; Raudsepp, M. Static tests of neutralization potentials of silicate and aluminosilicate minerals. *Environ. Geol.* **2002**, *43*, 1–17.
45. Ruan, R.; Zhou, E.; Xingyu, L.; Biao, W.; Guiying, Z.; Jiankang, W. Comparison on the leaching kinetics of chalcocite and pyrite with or without bacteria. *Rare Metals.* **2010**, *29*, 552–556.
46. Plante, B.; Bussière, B.; Benzaazoua, M. Static tests response on 5 Canadian hard rock mine tailings with low net acid-generating potentials. *J. Geochem. Explor.* **2012**, *114*, 57–69.
47. Banwart, S.A.; Destouni, G.; Malmström, M. Assessing mine water pollution: From laboratory to field scale. In *Ground Water Quality: Remediation and Protection, Proceeding of the GQ’98 Conference, Tübingen, Germany, 21–25 September 1998*; IAHS Publications: Wallingford, UK, 1998; Volume 250, pp. 307–311.
48. Pharaoh, T.C.; MacIntyre, R.M.; Ramsay, D.M. K–Ar age determination on the Raipas suite in the Komagfjord Window, northern Norway. *Nor. Geol. Tidsskr.* **1982**, *62*, 51–57.

49. Torgersen, E.; Viola, G.; Sandstad, J.S. Revised structure and stratigraphy of the northwestern Repparfjord Tectonic Window, Northern Norway. *Norw. J. Geol.* **2015**, *95*, 397–421.
50. Perelló, J.; Clifford, J.A.; Creaser, R.A.; Valencia, V.A. An example of synorogenic sediment-hosted copper Mineralization: Geological and geochronologic evidence from the Paleoproterozoic Nussir deposit, Finnmark, Arctic Norway. *Econ. Geol.* **2015**, *110*, 677–689.
51. Torgersen, E.; Viola, G.; Sandstad, J.S.; Stein, H.; Zwingmann, H.; Hannah, J. Effects of frictional–viscous oscillations and fluid flow events on the structural evolution and Re–Os pyrite–chalcopyrite systematics of Cu-rich carbonate veins in northern Norway. *Tectonophysics* **2015**, *659*, 70–90.
52. Torgersen, E.; Viola, G.; Sandstad, J.S.; Stein, H. Structural constraints on the formation of Cu-rich mesothermal vein deposits in the Repparfjord Tectonic Window, northern Norway. In Proceedings of the 12th SGA Biennial Meeting, Uppsala, Sweden, 12–15 August 2013.
53. Mun, Y.; Strmić Palinkaš, S.; Forwick, M.; Junttila, J.; Pedersen, K.B.; Sternal, B.; Neufeld, K.; Tibljaš, D.; Kullerud, K. Stability of Cu-sulfides in submarine tailing disposals: A case study from Repparfjorden, northern Norway. *Minerals* **2020**, *10*, 169, doi:10.3390/min10020169.
54. Stribny, B. The conglomerate-hosted Repparfjord copper ore deposit, Finnmark, Norway. In *Monograph Series on Mineral Deposits*; Gebrüder Borntraeger: Berlin, Germany; Stuttgart, Germany, 1985; Volume 24, pp. 1–75.
55. Mun, Y.; Strmić Palinkaš, S.; Kullerud, K.; Nilsen, K.S.; Neufeld, K.; Bekker, A. Evolution of metal-bearing fluids at the Nussir and Ulveryggen sediment-hosted Cu deposits, Repparfjord Tectonic Window, Northern Norway. *Norw. J. Geol.* **2020**, *100*, doi:10.17850/njg100-2-5.
56. Norwegian Geological Survey, available online: www.ngu.no (accessed on 12 October 2020).
57. Ettner, D. Passive mine water treatment in Norway. In *Water in Mining Environments*; Cidu, R., Frau, F., Eds.; IMWA Symposium; Cagliari, Italy, 2007.
58. Rui, I.J.; Bakke, I. Stratabound sulphide mineralization in the Kjølø Area, Røros District, Norwegian Caledonides. *Nor. Geol. Tidsskr.* **1975**, *55*, 51–75.
59. Bjerkgård, T.; Sandstad, J.S.; Sturt, B.A. Massive sulphide deposits in the south-eastern Trondheim region Caledonides, Norway: A review. In *Mineral Deposits: Processes to Processing*; Stanley, C.J., Ed.; Taylor & Francis: London, UK, 1999; pp. 935–938.
60. Grenne, T.; Ihlen, P.M.; Vokes, F.M. Scandinavian Caledonide metallogeny in a plate tectonic perspective. *Miner. Deposita* **1999**, *34*, 422–471.
61. Gee, D.G.; Fossen, H.; Henriksen, N.; Higgins, A.K. From the early Paleozoic platforms of Baltica and Laurentia to the Caledonide Orogen of Scandinavia and Greenland. *Episodes* **2008**, *31*, 44–51.
62. Corfu, F.; Andersen, T.B.; Gasser, D. The Scandinavian Caledonides: Main features, conceptual advances and critical questions. *Geol. Soc. Lond. Spec. Publ.* **2014**, *390*, 9–43.
63. RRUF project, available online: <https://truff.info/> (accessed on 2 February 2021).
64. Miljødirektoratet. *Quality Standards for Water, Sediment and Biota*; M-608; Norwegian Environment Agency (NEA): Oslo, Norway, 2016; 24p. (In Norwegian)
65. Barrie, C.T.; Hannington, M.D. Classification of volcanic-associated massive sulfide deposits based on host-rock composition. In *Volcanic-Associated Massive Sulfide Deposits: Processes and Examples in Modern and Ancient Settings*; Barrie, C.T., Ed.; Society of Economic Geologists: Littleton, CO, USA, 1999; pp. 1–11.
66. Galley, A.G.; Hannington, M.D.; Jonasson, I.R. Volcanogenic massive sulphide deposits. In *Mineral Deposits of Canada: A Synthesis of Major Deposit-Types, District Metallogeny, the Evolution of Geological Provinces, and Exploration Methods*; Goodfellow, W.D., Ed.; Geological Association of Canada, Mineral Deposits Division, Special Publication: St. John's, NL, Canada, 2007; Volume 5, pp. 141–161.
67. Nordstrom, D.K.; Alpers, C.N. Geochemistry of acid mine waters. In *The Environmental Geochemistry of Mineral Deposits, Part A. Processes, Techniques, and Health Issues*; Plumlee, G.S., Longsdon, M.J., Eds.; Society of Economic Geologists, Reviews in Economic Geology, Littleton, CO, USA; 1999; Volume 6A, pp. 133–160.
68. Hudson-Edwards, K.A.; Jamieson, H.E.; Lottermoser, B.G. Mine wastes: Past, present, future. *Elements* **2011**, *7*, 375–380.
69. Grimalt, J.O.; Ferrer, M.; Macpherson, E. The mine tailing accident in Aznacollar. *Sci. Total Environ.* **1999**, *242*, 3–11.
70. Levings, C.D.; Barry, K.L.; Grout, J.A.; Piercey, G.E.; Marsden, A.D.; Coombs, A.P.; Mossop, B. Effects of acid mine drainage on the estuarine food web, Britannia Beach, Howe Sound, British Columbia, Canada. *Hydrobiologia* **2004**, *525*, 185–202.
71. Parbhakar-Fox, A.K.; Lottermoser, B.; Bradshaw, D. Evaluating waste rock mineralogy and microtexture during kinetic testing for improved acid rock drainage prediction. *Miner. Eng.* **2013**, *52*, 111–124.
72. McKibben, M.A.; Tallant, B.A.; del Angel, J.K. Kinetics of inorganic arsenopyrite oxidation in acidic aqueous solutions. *Appl. Geochem.* **2008**, *23*, 121–135.
73. Temminghoff, E.J.M.; Van Der Zee, S.E.A.T.M.; De Haan, F.A.M. Copper mobility in a copper-contaminated sandy soil as affected by pH and solid and dissolved organic matter. *Environ. Sci. Technol.* **1997**, *31*, 1109–1115.
74. Balci, N.; Demirel, C. Prediction of acid mine drainage (AMD) and metal release sources at the Küre copper mine site, Kastamonu, NW Turkey. *Mine Water Environ.* **2017**, *37*, 56–74, doi:10.1007/s10230-017-0470-4.
75. Pareuil, P.; Pénilla, S.; Ozkan, N.; Bordas, F.; Bollinger, J.-C. Influence of reducing conditions on metallic elements released from various contaminated soil samples. *Environ. Sci. Technol.* **2008**, *42*, 7615–7621.

76. Engineering ToolBox. Oxygen—Solubility in Fresh Water and Seawater. 2005. Available online: https://www.engineeringtoolbox.com/oxygen-solubility-water-d_841.html (accessed on 4 May 2021).
77. Chizhikov, D.M.; Kovylyna, V.N. Investigation of potentials and anodic polarization of the sulfides and their alloys. In *Trudy Chetvertogo Soveshchaniya po Elektrokhimii Akademii Nauk SSSR, Proceedings of the 4th Conference on Electrochemistry*; Akademii Nauk SSSR, Frumkin, A.S. (Ed.): Moscow, Russia, 1–6 October, 1956; pp. 715–719.
78. Biegler, T.; Swift, D.A. Anodic behaviour of pyrite in acid solutions. *Electrochem. Acta* **1979**, *24*, 415–422.
79. Warren, G.W. The Electrochemical Oxidation of CuFeS₂. Ph.D. Thesis, University of Utah, Salt Lake City, UT, USA, 1978.
80. Ziemkiewicz, P.; Skousen, J.G. Open limestone channels for treating acid mine drainage: A new look at an old idea. *Green Lands* **1994**, *24*, 36–41.
81. Selvarajan, P.; Chandra, G.; Bhattacharya, S.; Sil, S.; Vinu, A.; Umapathy, S. Potential of Raman spectroscopy towards understanding structures of carbon-based materials and perovskites. *Emergent Mater.* **2019**, *2*, 417–439.